

Anomalous conductivity tensor in the Dirac semimetal Na₃Bi

Jun Xiong¹, Satya Kushwaha², Jason Krizan², Tian Liang¹, R. J. Cava², and N. P. Ong¹
Departments of Physics¹ and Chemistry², Princeton University, Princeton, NJ 08544

(Dated: October 31, 2016)

Na₃Bi is a Dirac semimetal with protected nodes that may be sensitive to the breaking of time-reversal invariance in a magnetic field \mathbf{B} . We report experiments which reveal that both the conductivity and resistivity tensors exhibit robust anomalies in B . The resistivity ρ_{xx} is B -linear up to 35 T, while the Hall angle exhibits an unusual profile approaching a step-function. The conductivities σ_{xx} and σ_{xy} share identical power-law dependences at large B . We propose that these significant deviations from conventional transport result from an unusual sensitivity of the transport lifetime to B . Comparison with Cd₃As₂ is made.

PACS numbers: 72.15.Gd, 72.20.My, 75.47.De, 72.80.Vp

In Dirac semimetals – the analogs of graphene in three-dimensional material – the bulk Dirac node is protected against gap-formation via hybridization. The iridate pyrochlores were initially predicted [1] to have protected nodes, but crystal growth has been problematical. Recently, Young *et al.* [2] identified a class of materials in which time-reversal invariance (TRI) leads to node protection when the nodes occur at high-symmetry points (the time-reversal invariant momenta or TRIM). Subsequently, Wang *et al.* proposed that crystalline symmetry can protect Dirac nodes even when they occur away from TRIM. From band calculations, they identified Na₃Bi [3] and Cd₃As₂ [4] as Dirac semimetals. Photoemission [5–9] and scanning tunneling microscopy [10] recently confirmed that bulk Dirac nodes exist in both Na₃Bi and Cd₃As₂. Many groups [12–15] predict that, in Dirac and Weyl semimetals, charge pumping associated with the chiral anomaly can be observed in an intense magnetic field \mathbf{B} . We report experiments on Na₃Bi showing that, even at low B , the breaking of TRI leads to robust anomalies in the conductivity tensor which appears to originate from a strongly B -dependent transport lifetime $\tau_{tr}(B)$. Among the anomalies are a robust B -linear magnetoresistance and an unusual step-like field profile of the Hall angle $\tan\theta$. The quantum oscillations show that Fermi surface (FS) is comprised of two distinct valleys, i.e. the Fermi energy lies in the non-trivial gap-inverted regime.

Na₃Bi single crystals were crystallized from the Na-rich compositions (90 and 95%) tuned to preclude the formation of the superconductor NaBi as an impurity phase [17, 18] (growth details are published elsewhere). The crystal structure was confirmed by X-ray diffraction (the lattice structure is sketched in Fig. 1C). The deep-purple crystals grow with the largest facets normal to the c -axis (001). To avoid deterioration of the crystals (which fully oxidize within 30 s of exposure to air), we attached contacts with Ag epoxy to the crystals inside an Ar glove-box and then covered them with oil before transferring to the cryostat (see Supplement). The resistivity profile ρ vs. T is metallic (Fig. 1A) with residual values ranging from 1.72 to 87 $\mu\Omega\text{cm}$. The Hall resistivity ρ_{yx} is n -type and strictly B -linear (Fig. 1), with a

nearly T -independent Hall coefficient $R_H = \rho_{yx}/B$ ($\hat{\mathbf{x}}\|\mathbf{I}$ and $\hat{\mathbf{z}}\|\hat{\mathbf{c}}$, where \mathbf{I} is the current). Batch B and C samples were measured without post annealing, while G1 was post-annealed for 1 month. Table S1 in the Supplement lists the transport quantities measured in 8 samples.

Figure 1B plots the MR curves in Sample B6 for selected θ (the tilt angle between $\hat{\mathbf{c}}$ and the field $\mathbf{H} = \mathbf{B}/\mu_0$, with μ_0 the vacuum permeability). As shown by the fan pattern, the MR ratio $\rho_{xx}(B)/\rho_{xx}(0)$ decreases rapidly as \mathbf{H} is tilted into the a - b plane ($\theta \rightarrow 90^\circ$).

All the samples display prominent Shubnikov de Haas (SdH) oscillations in $\rho_{xx}(B)$, from which the Fermi Surface cross-section S_F and the Fermi wavevector k_F are determined. In addition, we have measured the de Haas van Alven (dHvA) oscillations using torque magnetometry. Figure 2A shows the oscillatory component of the magnetization together with a fit to the Lifshitz-Kosevich (LK) expression. From fits to the dHvA amplitudes vs. $1/H$ and T (Panels B and C), we determine the effective mass m^* , the Fermi velocity v_F and the quantum lifetime τ_Q . The carrier density $n = g_v k_F^3/3\pi^2$ (with the valley and spin degeneracies g_v and g_s both equal to 2) ranges from 2.6 - $4.1 \times 10^{19} \text{ cm}^{-3}$, consistent with the Hall effect (Table S1). In addition, by varying θ in the MR, we verify that the FS cross section S_F is nearly spherical (Fig. 2D).

Because of unintentional doping from vacancies, the Fermi energy E_F is in the conduction band, as implied by the n -type sign of the Hall resistivity ρ_{yx} . The band calculations [3] predicted the existence of two Dirac nodes centered at $(0, 0, \pm k_D)$ caused by gap inversion (sketch in Fig. 2D). As E_F rises in the conduction band, the two Dirac cones merge into a single cone when E_F exceeds the Lifshitz-transition energy E_L . Recent ARPES experiments have confirmed the predicted dispersion and measured k_D to be 0.095 \AA^{-1} [5] and 0.10 \AA^{-1} [9] (see also [19]). An important issue is whether E_F in our samples lies above or below E_L . As shown in Table S1, our measured k_F ranges from 0.073 to 0.084 \AA^{-1} . As these values are smaller than k_D , we conclude that E_F lies below E_L . The FS is comprised of two distinct valleys on opposite sides of Γ , i.e. $g_v = 2$. A persistent feature is a weak beating pattern in the SdH oscillations. Figure

3a shows the SdH traces from 5 samples. The Fourier spectra of the oscillations reveal two frequencies f_1 and f_2 corresponding to two values of S_F differing by $\sim 16\%$. The beating suggests that the orbits may reflect quantum interference between the two orbits. We hope to explore the beating in high-mobility crystals.

The mobility μ of each sample is directly measured from the field profile of the Hall conductivity σ_{xy} . As shown in Fig. 3b, $\sigma_{xy}(B)$ has the characteristic dispersion-resonance profile produced by cyclotron motion of the carriers. By the Bloch-Boltzmann theory, the extrema in $\sigma_{xy}(B)$ occur at the peak fields $\pm B_\mu$, with $1/B_\mu = \mu$. With increasing μ , from sample B10 ($\mu = 21,640 \text{ cm}^2/\text{Vs}$) to B6 ($39,250 \text{ cm}^2/\text{Vs}$) and G1 ($91,000 \text{ cm}^2/\text{Vs}$), the peak field B_μ systematically decreases. The variation in μ strongly influences the Hall-angle profile (see below). Using $\mu = ev_F\tau_{tr}/\hbar k_F$, we find that the transport lifetime τ_{tr} exceeds τ_Q by a ratio $R_\tau = 10\text{--}20$ (R_τ is expected to exceed 1 since τ_Q reflects broadening due to all scattering processes). In Cd_3As_2 , R_τ is as large as 10^4 [16].

In the relaxation-time *ansatz*, the Boltzmann equation describing changes to the distribution function $f_{\mathbf{k}}$ caused by an electric field \mathbf{E} is expressed as [11]

$$e\mathbf{E} \cdot \mathbf{v} \frac{\partial f_{\mathbf{k}}^0}{\partial E_{\mathbf{k}}} + e\mathbf{v} \times \mathbf{B} \cdot \frac{\partial g_{\mathbf{k}}}{\partial \mathbf{k}} = -\frac{g_{\mathbf{k}}}{\tau_{tr}}, \quad (1)$$

where e is the elemental charge and $g_{\mathbf{k}} = f_{\mathbf{k}} - f_{\mathbf{k}}^0$, with $f_{\mathbf{k}}^0$ the Fermi-Dirac function. $E_{\mathbf{k}}$ and velocity \mathbf{v} are, respectively, the energy and velocity at state \mathbf{k} . The *ansatz* yields the conductivity tensor σ_{ij} , with

$$\sigma_{xx} = ne\mu/D, \quad \sigma_{xy} = ne\mu^2 B/D, \quad (2)$$

where $D = 1 + (\mu B)^2$. From Eq. 2, the ratio $\sigma_{xy}/\sigma_{xx} = \mu B$, which is the Hall angle $\tan \theta$, is linear in B . By contrast, the resistivity ρ_{xx} is B -independent because the Hall electric-field E_y exactly balances the Lorentz force. Significantly, $\sigma_{xx} \sim 1/B^2$ decreases much faster than $\sigma_{xy} \sim 1/B$ when $\mu B \gg 1$. These standard predictions assume that τ_{tr} (hence μ) is a constant independent of B . In conventional metals and semimetals in the impurity-scattering regime (elastic scattering), this assumption is firmly established; the predicted trends are a cornerstone of semiclassical transport.

In Na_3Bi , however, the observed field dependences of the diagonal elements σ_{xx} and ρ_{xx} disagree in an essential way from the standard predictions (only $\rho_{yx}(B)$ appears conventional). As we noted in Fig. 1, the resistivity increases linearly with B instead of saturating. A B -linear MR is rare in conventional conductors (see Abrikosov's comments [20]; we exclude metals with open orbits [11]). However, in materials with unusual topological phases, a B -linear MR is increasingly encountered [21]. To persuade ourselves that the B -linear MR is pervasive in Na_3Bi , we have investigated 8 samples (Table S1). Figure 4A shows that the B -linear MR is a very robust feature in Na_3Bi . Across the samples, the MR ratio (measured

at 15 T) increases from ~ 14 in B10, to 163 in G1 (the sample with the highest μ). In B11, we show that the B -linear profile extends to 35 T with no evidence of deviation.

A second dramatic anomaly is seen in the Hall-angle profile. In Fig. 4B, we compare $\tan \theta$ measured in four samples with increasing μ , B10, B12, B6 and G1. As shown, $\tan \theta$ initially rises very rapidly in weak B at a rate dictated by the mobility, but saturates to a plateau value at large B . Whereas the saturation is gradual in the samples with low mobility (B10 and B12), the rise becomes abrupt in higher-mobility samples (B6 and G1). In G1, especially, the profile resembles a step-function profile. $\tan \theta$ assumes a virtually B -independent value from $B = 0.5$ to 15 T instead of increasing linearly with B . Since $\tan \theta = \mu B$, the simplest interpretation of the step-function profile is that, starting in weak B , the transport lifetime varies with B as

$$\tau_{tr} \sim 1/B. \quad (3)$$

The merit of Eq. 3 is that it also accounts for the B -linear MR profile, i.e. $\rho_{xx} = 1/ne\tau_{tr} \sim B$. Interestingly, with Eq. 3, the high-field B dependence of σ_{xx} is reduced by one power of B to $\sigma_{xx}(B) \sim 1/B$ (Eq. 2), but leaves that of $\sigma_{xy} \sim 1/B$ unchanged because μ cancels out at large B . Hence both σ_{xx} and σ_{xy} vary as $1/B$ at large B , consistent with the step-profile of $\tan \theta$.

To verify this, we plot the B dependences of σ_{xx} and σ_{xy} in log-log scale for the two high-mobility samples B6 and G1 (Fig. 5). In both samples, the two conductivities have the same power-law dependence $B^{-\beta}$ above a relatively low B . Consistent with the behavior of $\tan \theta$, this occurs at $B = 2$ T and 0.3 T in B6 and G1, respectively. The measured value of β is 1.0 in B6, but is slightly larger (1.15) in G1.

Theoretically, in the Weyl semimetal, the Weyl nodes which come in pairs act as sources and sinks of Berry curvature (Chern flux) [1, 12–15]. To realize a finite Berry curvature $\vec{\Omega}(\mathbf{k})$, TRI must be broken in the Weyl semimetal. The 3D Dirac semimetal may be regarded as the limiting case when TRI is restored. In this limit, the Weyl nodes coincide in \mathbf{k} space but are prevented from hybridizing by crystalline symmetry. Conversely [3], one expects that, in a Dirac semimetal, the breaking of TRI by an applied \mathbf{B} will render $\vec{\Omega}(\mathbf{k})$ finite, and lead to essential changes in its FS best detected by transport experiments.

To date, theoretical attention has focused on the charge-pumping of the chiral current from left to right-moving branches [12–15, 22]. However, as shown by the results here, the essential changes to the FS topology induced by \mathbf{B} should skew σ_{xx} and ρ_{xx} away from conventional behavior even in weak B . The results for Na_3Bi (and Cd_3As_2 [16]) invite a systematic re-examination of transport in Dirac semimetals. We compare the two materials in the Supplement.

* * *

We thank Andrei Bernevig and Ashvin Vishwanath for valuable discussions. N.P.O. is supported by the Army Research Office (ARO W911NF-11-1-0379). R.J.C. and N.P.O. are supported by a MURI grant on Topological Insulators (ARO W911NF-12-1-0461) and by the US National Science Foundation (grant number DMR 1420541).

T.L. acknowledges scholarship support from the Japan Student Services Organization. Some of the experiments were performed at the National High Magnetic Field Laboratory, which is supported by National Science Foundation Cooperative Agreement No. DMR-1157490, the State of Florida, and the U.S. Department of Energy.

-
- [1] X. G. Wan, A. M. Turner, A. Vishwanath and S. Y. Savrasov, "Topological semimetal and Fermi-arc surface states in the electronic structure of pyrochlore iridates," *Phys Rev B* **83**, 205101 (2011).
- [2] S. M. Young, S. Zaheer, J. C. Y. Teo, C. L. Kane, E. J. Mele and A. M. Rappe, "Dirac Semimetal in Three Dimensions," *Phys Rev Lett* **108**, 140405 (2012).
- [3] Z. J. Wang, Y. Sun, X. Q. Chen, C. Franchini, G. Xu, H. M. Weng, X. Dai and Z. Fang, "Dirac semimetal and topological phase transitions in A_3Bi ($A = Na, K, Rb$)," *Phys Rev B* **85**, 195320 (2012).
- [4] Z. J. Wang, H. M. Weng, Q. S. Wu, X. Dai and Z. Fang, "Three-dimensional Dirac semimetal and quantum transport in Cd_3As_2 ," *Phys Rev B* **88**, 125427 (2013).
- [5] Z. K. Liu, B. Zhou, Y. Zhang, Z. J. Wang, H. M. Weng, D. Prabhakaran, S. K. Mo, Z. X. Shen, Z. Fang, X. Dai, Z. Hussain and Y. L. Chen, "Discovery of a Three-Dimensional Topological Dirac Semimetal, Na_3Bi ," *Science* **343**, 864-867 (2014).
- [6] Madhab Neupane, Su-Yang Xu, Raman Sankar, Nasser Alidoust, Guang Bian, Chang Liu, Ilya Belopolski, Tay-Rong Chang, Horng-Tay Jeng, Hsin Lin, Arun Bansil, Fangcheng Chou and M. Zahid Hasan, "Observation of a three-dimensional topological Dirac semimetal phase in high-mobility Cd_3As_2 " *Nat. Commun.* **5**:3786 doi: 10.1038/ncomms4786 (2014).
- [7] Z. K. Liu, J. Jiang, B. Zhou, Z. J. Wang, Y. Zhang, H. M. Weng, D. Prabhakaran, S-K. Mo, H. Peng, P. Dudin, T. Kim, M. Hoesch, Z. Fang, X. Dai, Z. X. Shen, D. L. Feng, Z. Hussain, and Y. L. Chen, "A stable three-dimensional topological Dirac semimetal Cd_3As_2 ," *Nat. Mater.* **13**, 677-681 (2014).
- [8] Sergey Borisenko, Quinn Gibson, Danil Evtushinsky, Volodymyr Zabolotnyy, Bernd Böhner, and Robert J. Cava, "Experimental Realization of a Three-Dimensional Dirac Semimetal," *Phys. Rev. Lett.* **113**, 027603 (2014).
- [9] S.-Y. Xu, C. Liu, S. K. Kushwaha, T.-R. Chang, J. W. Krizan, R. Sankar, C. M. Polley, J. Adell, T. Balasubramanian, K. Miyamoto, N. Alidoust, G. Bian, M. Neupane, I. Belopolski, H.-T. Jeng, C.-Y. Huang, W.-F. Tsai, H. Lin, F. C. Chou, T. Okuda, A. Bansil, R. J. Cava, M. Z. Hasan, "Observation of a bulk 3D Dirac multiplet, Lifshitz transition, and nested spin states in Na_3Bi ," *arXiv:1312.7624* (2013)
- [10] Sangjun Jeon, Brian B. Zhou, Andras Gyenis, Benjamin E. Feldman, Itamar Kimchi, Andrew C. Potter, Quinn D. Gibson, Robert J. Cava, Ashvin Vishwanath, and Ali Yazdani, "Landau quantization and quasiparticle interference in the three-dimensional Dirac semimetal Cd_3As_2 ," *Nat. Mater.* **13**, 851-856 (2014).
- [11] J. M. Ziman, "Electrons and Phonons," (Oxford Univ. Press, London, 1960).
- [12] D. T. Son and B. Z. Spivak, "Chiral anomaly and classical negative magnetoresistance of Weyl metals," *Phys Rev B* **88**, 104412 (2013).
- [13] A. A. Burkov, M. D. Hook and L. Balents, "Topological nodal semimetals," *Phys Rev B* **84**, 235126 (2011).
- [14] Pavan Hosur and Xiaoliang Qi "Recent developments in transport phenomena in Weyl semimetals," *arXiv:1309.4464*
- [15] S.A. Parameswaran, T. Grover, D. A. Abanin, D. A. Pesin, A. Vishwanath, "Probing the Chiral Anomaly with Nonlocal Transport in Three-Dimensional Topological Semimetals", *Phys. Rev. X* **4**, 031035 (2014).
- [16] Tian Liang, Quinn Gibson, Mazhar N. Ali, Minhao Liu, R. J. Cava and N. P. Ong, "Ultrahigh mobility and giant magnetoresistance in Cd_3As_2 : protection from backscattering in a Dirac semimetal," submitted, *cond-mat arXiv:1404.7794*
- [17] S K Kushwaha, J W Krizan, J Xiong, T Klimczuk, Q D Gibson, T Liang, N P Ong and R J Cava, *J. Phys. Condens. Matter* **26**, 212201 (2014).
- [18] G. Brauer and E. Zintl, "Konstitution von Phosphiden, Arsoniden, Antimoniden und Wismutiden des Lithiums, Natriums und Kaliums," *Z. Phys. Chem., Abt. B* **37**, 323-352 (1937).
- [19] Yi Zhang, Zhongkai Liu, Bo Zhou, Yeongkwan Kim, Zahid Hussain, Zhi-Xun Shen, Yulin Chen, and Sung-Kwan Mo, "Molecular beam epitaxial growth of a three-dimensional topological Dirac semimetal Na_3Bi ," *Appl. Phys. Lett.* **105**, 031901 (2014)
- [20] A. A. Abrikosov, "Quantum magnetoresistance," *Phys Rev B* **58**, 2788-2794 (1998).
- [21] D. X. Qu, Y. S. Hor, J. Xiong, R. J. Cava and N. P. Ong, "Quantum Oscillations and Hall Anomaly of Surface States in the Topological Insulator Bi_2Te_3 ," *Science* **329**, 821-824 (2010).
- [22] H. B. Nielsen and M. Ninomiya, "The Adler-Bell-Jackiw Anomaly and Weyl Fermions in a Crystal," *Phys Lett B* **130**, 389-396 (1983).

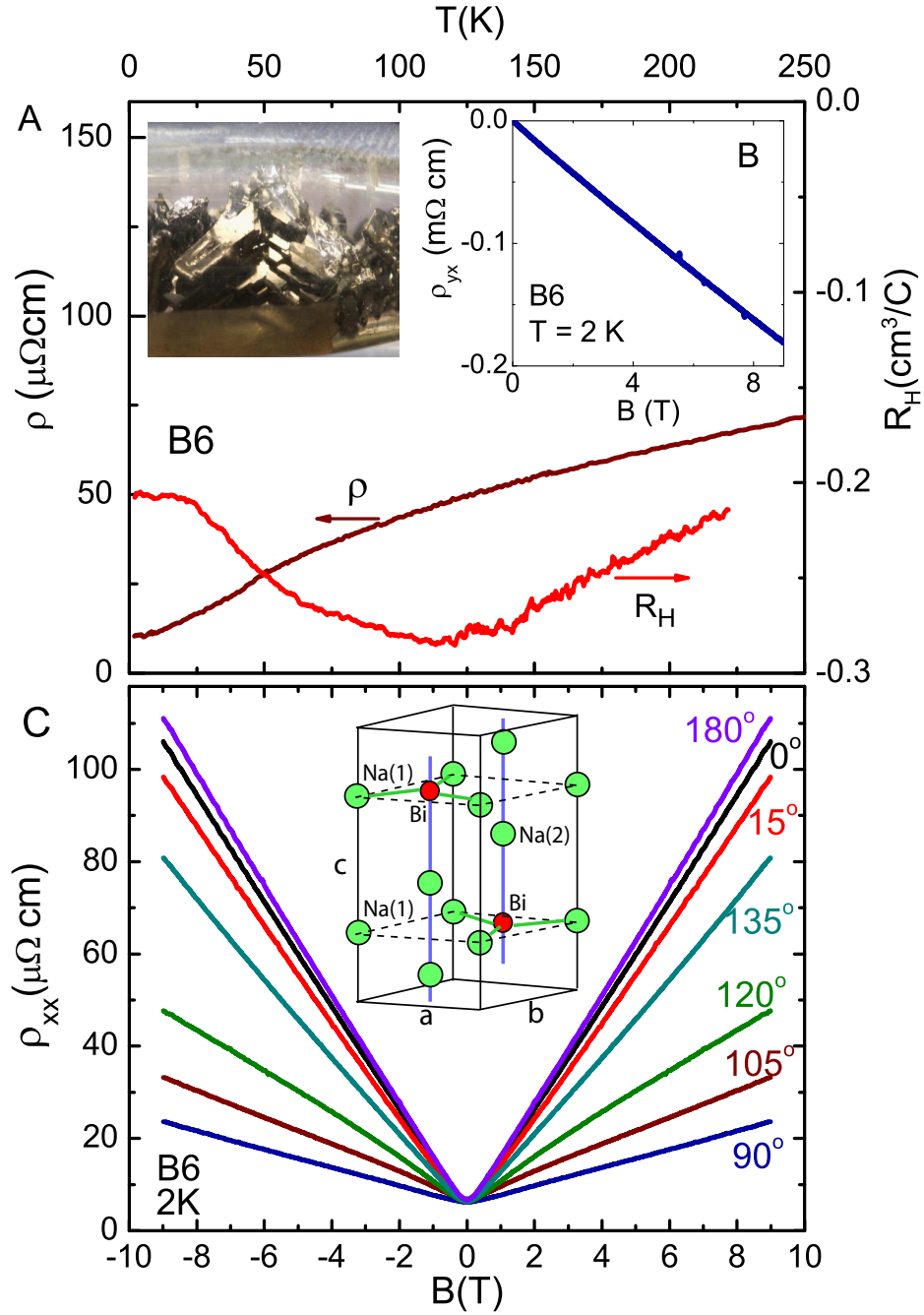


FIG. 1: (Color online) Magnetotransport in Na₃Bi. Panel A: The zero-field resistivity ρ and the Hall coefficient R_H vs. T (measured with $\mathbf{H}||\hat{c}$). Inset shows the crystals sealed in a vial. The largest facet is normal to \hat{c} . Panel (B) shows the Hall resistivity ρ_{yx} vs. B measured at 2 K in B6. Panel (C): The H -linear magnetoresistance in Sample B6 measured at 2 K at selected tilt angles θ to \hat{c} . The MR ratio is largest at $\theta = 0^\circ$ (and 180°). ($\mathbf{B} = \mu_0\mathbf{H}$ with μ_0 the vacuum permeability). The crystal structure of Na₃Bi is sketched in the inset (adapted from Ref. [5]).

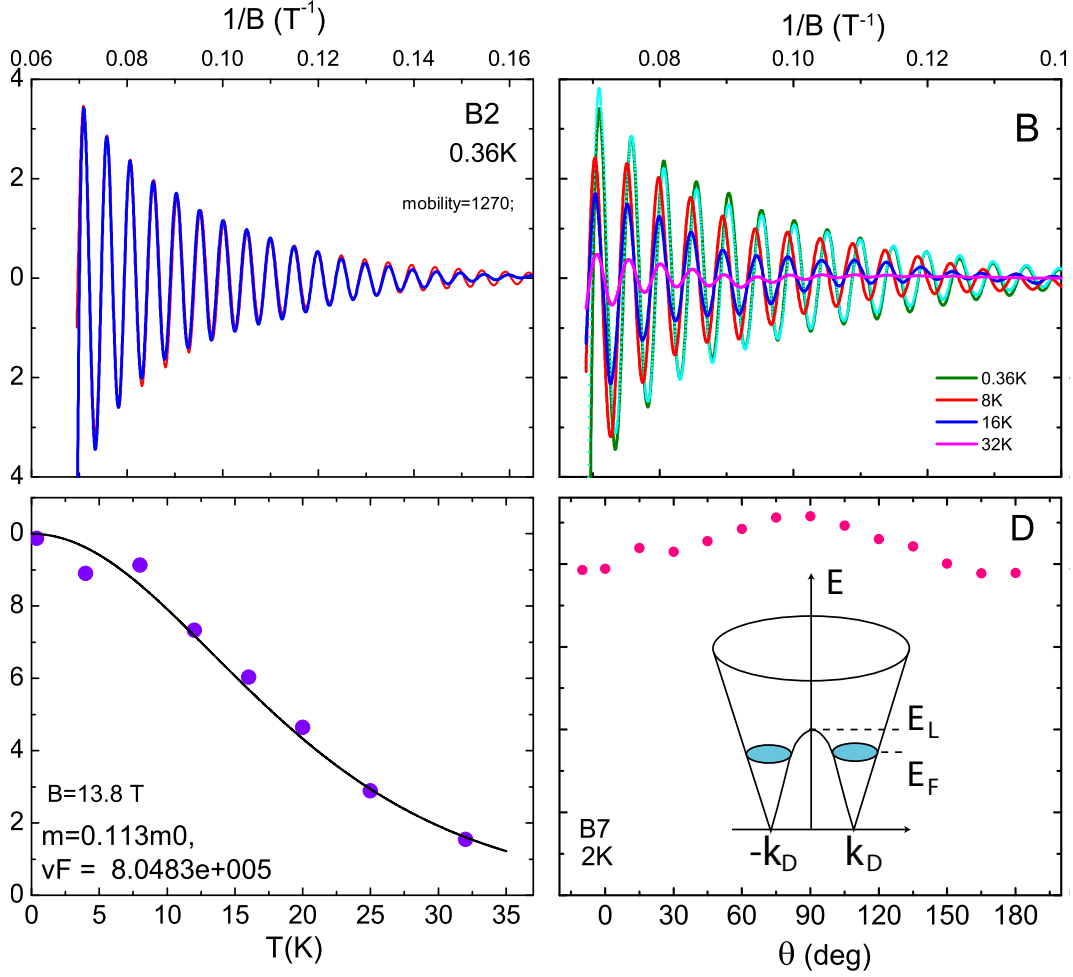


FIG. 2: (Color online) Torque measurements of the de-Haas van Alven (dHvA) oscillations in Na₃Bi. The dHvA oscillations (solid curve in Panel A) can be fit well to the LK expression (dashed curve) with one period. From the damping versus H (Panel A) and the T dependence (Panels B and C), we obtain the Fermi surface section S_F , the effective mass $m^* = 0.11m_0$ (m_0 the free mass), velocity $v_F = 8.05 \times 10^5$ m/s, and $\tau_Q = 8.16 \times 10^{-14}$ s. The plot of the peak fields B_{min} and B_{max} vs. the integers N (Panel D) yields S_F .

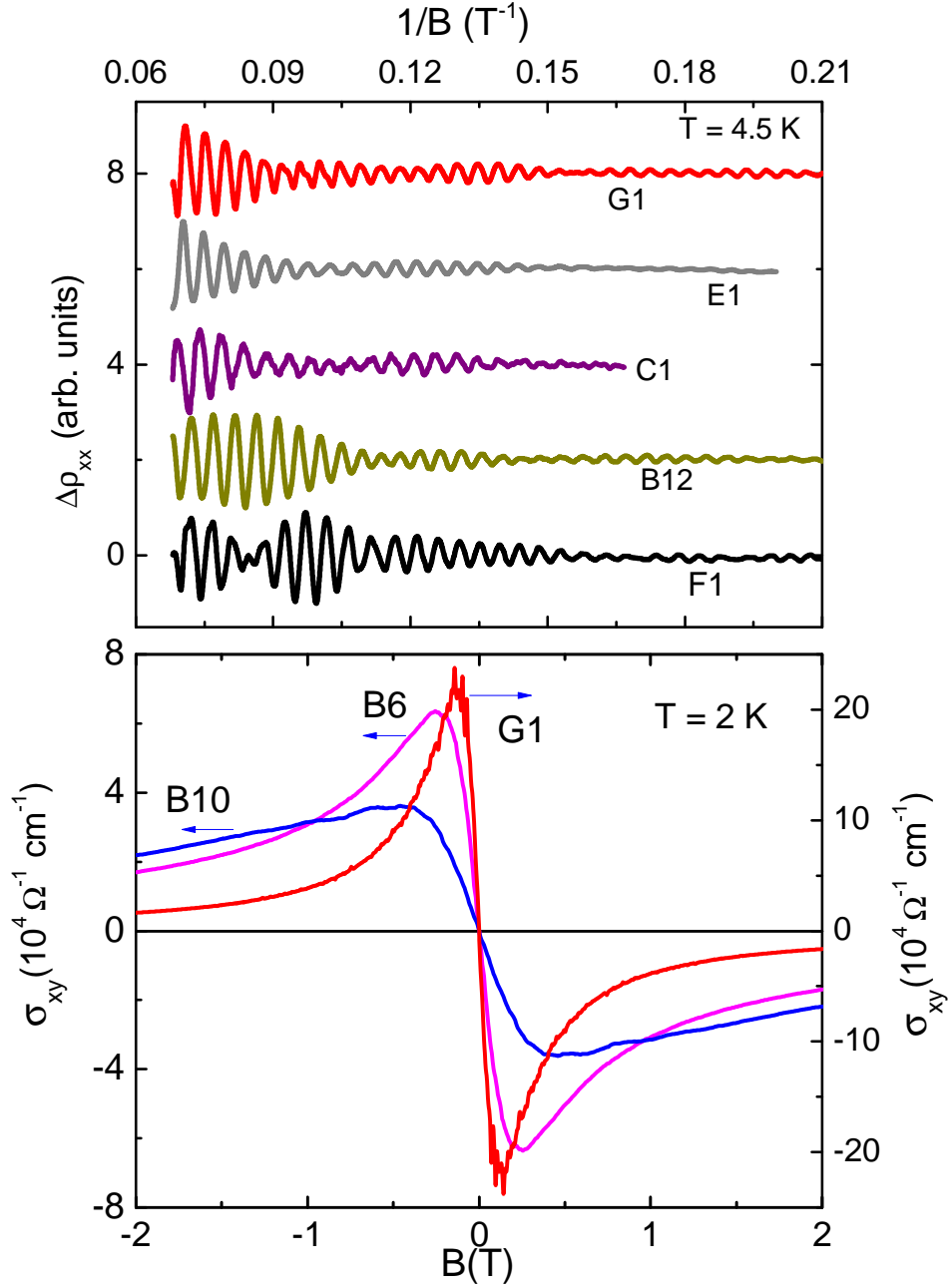


FIG. 3: (Color online) Panel A: Curves of $\Delta\rho_{xx}$ showing modulation of the SdH amplitude. The beating pattern implies a small splitting of the fundamental SdH frequency. Panel B compares the Hall conductivity $\sigma_{xy}(B)$ in 3 samples at 2 K. In the 3 curves, the peak field $\pm B_\mu$ yields the values $\mu = 21,640, 39,250$ and $91,000$ cm^2/Vs in B10, B6 and G1, respectively.

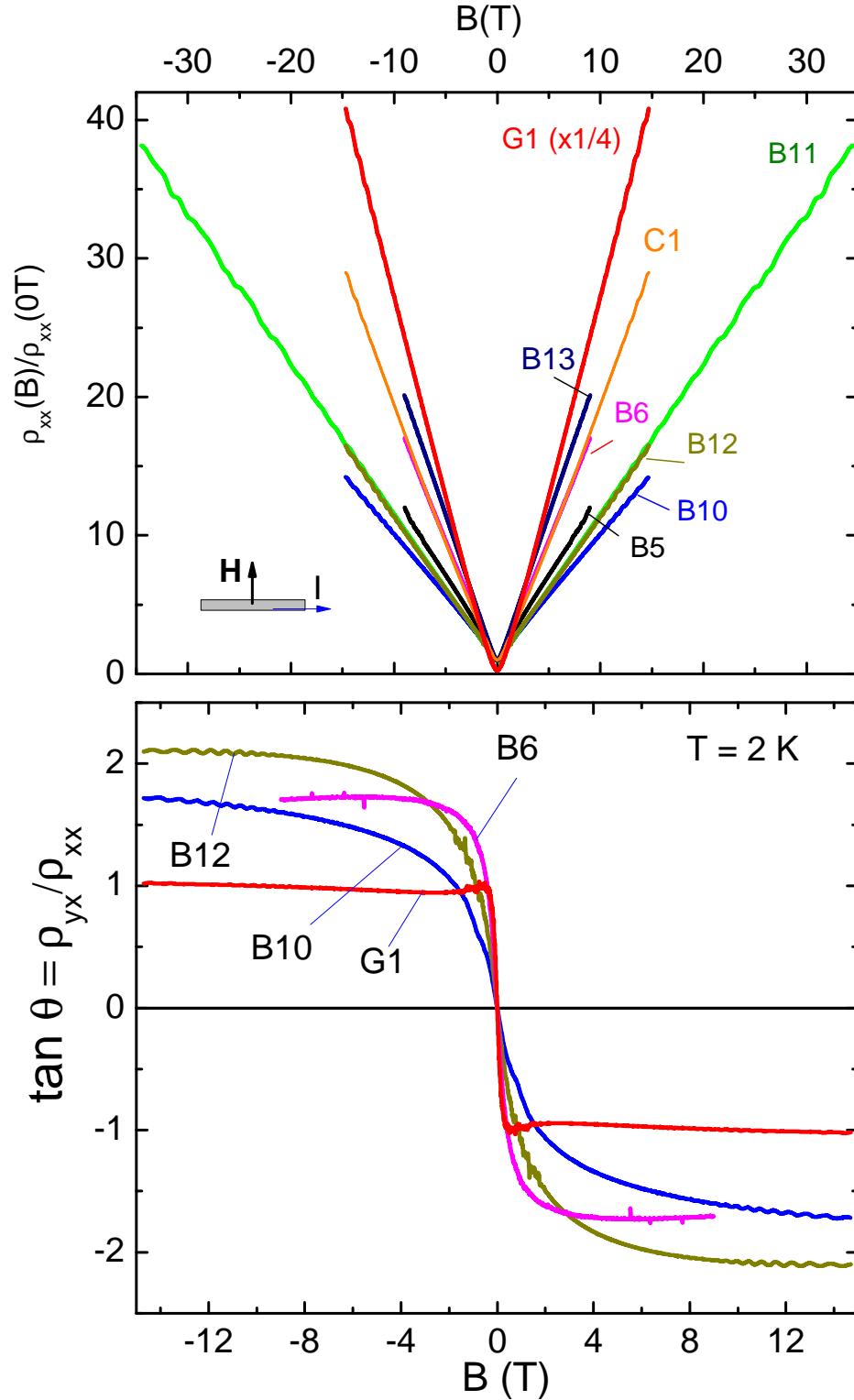


FIG. 4: (Color online) Robust H -linear magnetoresistance in Na₃Bi (Panel A). In the 8 samples shown, $\rho_{xx}(B)$ is measured with $\mathbf{H}||\hat{c}$ at 2 K in all cases except in B11 (at 1.6 K). In B11, the MR persists without observable deviation to 35 T. A general trend is that the MR increases with μ , from ~ 14 (at 15 T) in B10, to ~ 160 in G1 (which has the highest μ) (the MR in G1 is plotted in $\frac{1}{4}$ scale). In Panel B, the field profile of $\tan \theta = \rho_{yx}/\rho_{xx}$ is compared in 4 samples. As H increases, $\tan \theta$ rapidly saturates to an H -independent value, which implies the anomalous relationship $\tau_{tr} \sim 1/H$. In G1, the change occurs at 0.5 T.

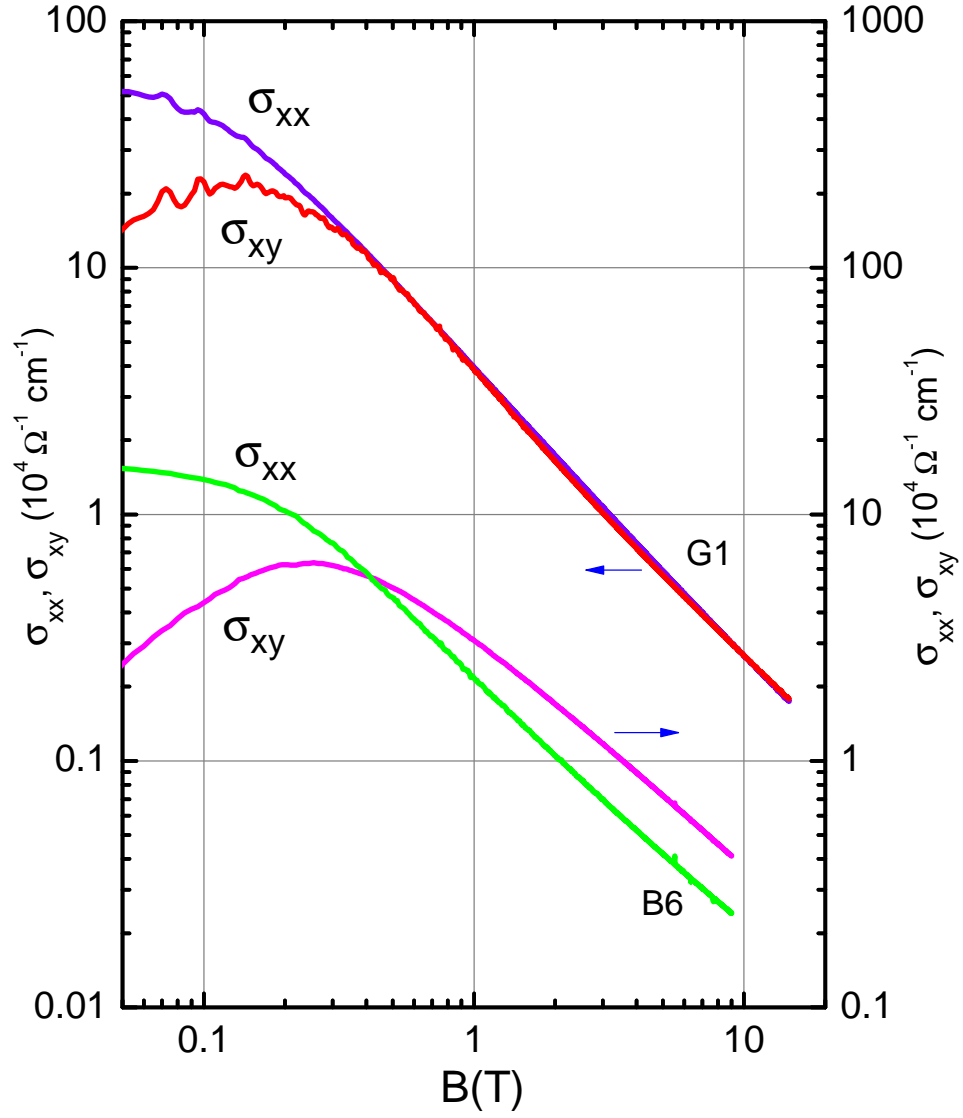


FIG. 5: (Color online) Log-log plots of σ_{xx} and σ_{xy} vs. B in G1 and B6. Consistent with Eq. 3, both quantities approach the same power law $B^{-\beta}$ when B exceeds 0.3 and 2 T in G1 and B6, respectively. The measured β is 1.15 and 1.0 in G1 and B6, respectively. Curves for B6 are shifted vertically.